Impacts of non-plane waves on two-station measurements of phase velocities

Helle A. Pedersen

Geophys. J. Int. (2006) **165,** 279–287 doi: 10.1111/j.1365-246X.2006.02893.x

Impacts of non-plane waves on two-station measurements of phase velocities

Helle A. Pedersen[1,2,3]

[1] *Laboratoire de Géophysique Interne et Tectonophysique, Grenoble University,* BP 53, F-38041 *Grenoble, France. E-mail: helle.pedersen@obs.ujf-grenoble.fr*
[2] *GeoForschungsZentrum Potsdam, Germany*
[3] *University of Potsdam, Potsdam, Germany*

Accepted 2005 December 16. Received 2005 December 13; in original form 2005 February 9

SUMMARY

To determine the regional shear wave velocities in the lithosphere it is frequently necessary to use two-station dispersion curves. We investigate the influence of non-plane wave energy on such dispersion curves, and compare them to two other better known sources of error: deviations from great-circle paths and uncorrelated noise. To study the influence of non-plane waves created from distant heterogeneities we create complex wavefields in a laterally homogeneous medium by adding interfering waves to a main plane wave. We then calculate the apparent phase velocity between two seismic stations located 100–400 km apart. Using realistic values for the sources of error, we conclude that the contribution of each is similar for 200-km-long profiles. Our conclusions on non-plane waves are made under the assumption that non-plane energy from distant heterogeneities varies randomly with hypocentre location. If this is correct, then only five to 10 events with different hypocentres are required to obtain a stable dispersion curve with less than 1 per cent error. The influence of uncorrelated noise and non-plane waves diminish for longer profiles, while the errors due to great-circle deviations are independent of profile length and systematically bias the dispersion curve to higher velocities. We recommend the inclusion of some off-profile broad-band stations for surface wave studies on a regional scale, because such supplementary stations make it possible to apply first-order corrections for off great-circle propagation. The strong influence from the different sources of error, combined with our lack of precise knowledge of the nature and amplitude of non-plane energy, implies that the interpretation of two-station measurements should be restricted to major changes in regional earth structure.

Key words: lithosphere, seismic velocities, seismic wave propagation, surface waves.

1 INTRODUCTION

With the increasing number of broad-band sensors available for temporary field experiments, it is becoming feasible to analyse teleseismic surface waves on a regional scale using techniques that require a large number of seismic stations in a 2-D array (e.g. Friederich 1998; Pollitz 1999; Li *et al.* 2003; Bruneton *et al.* 2004). Such techniques make it possible to include different aspects of local diffraction and in particular to take into account non-plane incident wavefields. Many temporary passive seismic experiments still have a relatively low number of broad-band sensors (to approximately 100 s period) or use sensors located along an essentially linear profile. In such cases, which are the focus of this study, the only possible approach for teleseismic surface wave analysis is to perform some kind of two-station measurements, combined when appropriate with simple tomography techniques.

Since Wielandt (1993) formalized the concept that surface wave fronts generally do not propagate with the so-called 'structural velocity', that is, the velocity predicted from the local modes of the underlying structure (Maupin 1988), several authors have questioned the validity of two-station measurements (e.g. Friederich *et al.* 1994, 2000). Here we only summarize the main issues pertaining to non-plane wave fronts, and refer the reader to the papers by Friederich *et al.* for more detailed information.

Non-plane incoming waves create a wavefield that has varying amplitudes and oscillating phases. Non-plane waves can be viewed as a summation of plane waves of varying amplitude and propagation direction, and it is the interference of these waves that creates the varying amplitudes and phases. The resulting wave front advances with a dynamic velocity that can be significantly different from the structural velocity, even when the amplitude of the non-plane energy is small.

The non-plane energy is created by the diffraction of surface waves in a laterally heterogeneous medium. Surface wave diffraction has already received considerable attention over the last several decades, (e.g. McGarr & Alsop 1967) and a complete review is not

appropriate here. The difficulty with surface wave diffraction resides in the strong coupling between modes and wave types, and the complex relationship that exists between such conversions and Earth heterogeneities (e.g. Gregersen 1978; Kennett 1984; Snieder 1986; Nolet 1987; Maupin 1988; Marquering *et al.* 1996; Pedersen *et al.* 1996; Maupin 2001; Yoshizawa & Kennett 2002). We do not yet understand all the phenomena related to surface wave diffraction, and we cannot yet invert for surface waveforms without introducing model smoothing and applying some approximation to the wave equation.

Independent of the origin of the non-plane energy, it is theoretically possible to calculate the structural velocity from the dynamic velocity using a corrective term that uses the second spatial derivatives of the natural logarithm of the wave amplitude (Wielandt 1993). However, this correction is unrealistic in practice due to insufficient station density. Even when many stations are available it is only possible to recover relatively smoothly varying wave fronts (e.g. Friederich 1998; Pollitz 1999; Bruneton *et al.* 2004).

We here focus on two-station phase velocity measurements as this is the standard way to estimate the absolute *S*-wave structure between pairs of seismic broad-band stations. For such measurements the magnitude of the errors induced by non-plane waves remains uncertain. It is also unclear whether averaging over a large number of events is sufficient to determine a phase velocity that is close to the average structural velocity between the two stations. If two-station measurements do not give useful results due to non-plane energy, it then serves no purpose to include small numbers of broad-band sensors in temporary field experiments.

The scope of this paper is to determine the stability of two-station dispersion curves in the presence of non-plane wave energy, independently of how this energy is created. We will represent this non-plane energy as a sum of random plane waves. This statistical approach is equivalent to assuming that non-plane energy is not dominated by heterogeneities close to, or within, the area in which the seismic stations are located. This assumption is unlikely to be valid within regions of strong lateral heterogeneity. The determination of local 3-D heterogeneous structure by analysis of teleseismic surface waves requires the use of a 2-D broad-band network (e.g. Friederich 1998; Pollitz 1999; Li *et al.* 2003; Bruneton *et al.* 2004). In this paper we assume that a 2-D network is not available and that we are required to use two-station measurements.

Whether or not two-station phase velocities are indicative of the average structure beneath the station profile in the presence of local heterogeneities, depends on (a) the exact 3-D earth structure, (b) the station locations within the structure and (c) the incidence direction of the surface waves (e.g. Pedersen *et al.* 1996). With improved tools for calculation of seismic wave propagation in 3-D heterogeneous earth models, it will soon be feasible to carry out such case studies for a given field experiment. Here we focus on general conclusions concerning the errors due to non-plane waves created at some distance to the array. To estimate the significance of these errors, we compare their effects to those of deviations from great-circle paths and uncorrelated noise.

2 DEVIATIONS FROM GREAT-CIRCLE PROPAGATION

Deviations from great-circle propagation can be very difficult to estimate at individual stations due to the complexity of the wavefield. Array analysis of 20–100 s period waves in the French Alps (Cotte *et al.* 2000) showed that the deviations may be greater than 30°. Cotte *et al.* (2000) used ray tracing (Woodhouse & Wong 1986) to predict angular deviations of 35s surface waves. They predicted that large-scale earth structures account for approximately ±20° while the local structure was responsible for another ±10°–15°. Alsina & Snieder (1996) observed strong deviations at a broad-band array in Netherlands, while smaller deviations were observed in the Iberian Peninsula (Alsina *et al.* 1993).

In cases where source–receiver paths are employed for surface wave tomography, it is possible to use observed deviations from the great-circle paths to further constrain earth models (e.g. Laske & Masters 1996; Yanovskaya 1996; Yoshizawa *et al.* 1999). In such cases, ray tracing can be included in the inversion (e.g. Laske & Masters 1996; Kennett & Yoshizawa 2002). However, for local two-station measurements the deviations can only be considered as noise as they are dominated by the earth structure outside the study area.

In absence of great-circle deviations, the velocity $C(f)$ between two stations is given by

$$C(f) = \frac{D\cos(\alpha)}{\Delta t(f)} \tag{1}$$

where f is frequency, Δt is the difference of arrival times of the wave at the two stations, D is the interstation distance, and α is the angle between the station profile and the great-circle (see Fig.1a). $D\cos(\alpha)$ is the length of the projection of the station profile onto

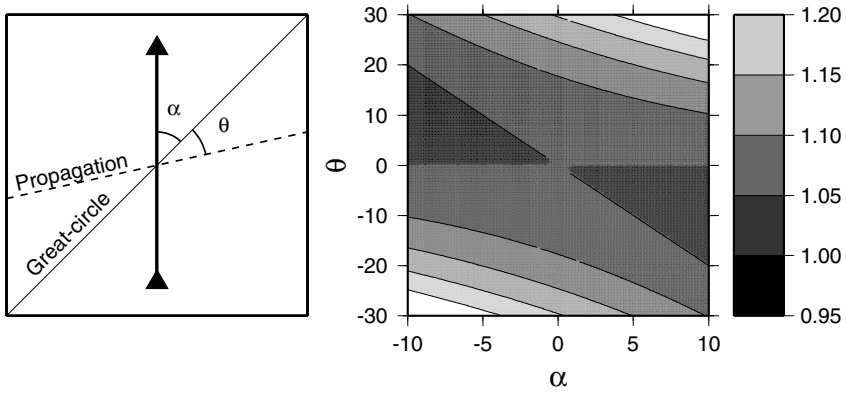

Figure 1. Influence of great-circle deviations upon apparent phase velocities. Left: Definition of the geometry. The triangles show the stations which define the station profile (bold line). α is the angle in degrees between the station profile and the great-circle, shown by the thin line. θ is the angle in degrees that defines the great-circle deviation, that is, the angle between the great-circle and wave propagation direction (or slowness vector), shown as a dashed line. Right: The ratio between apparent C_{app} and structural C phase velocity as a function of α and θ.

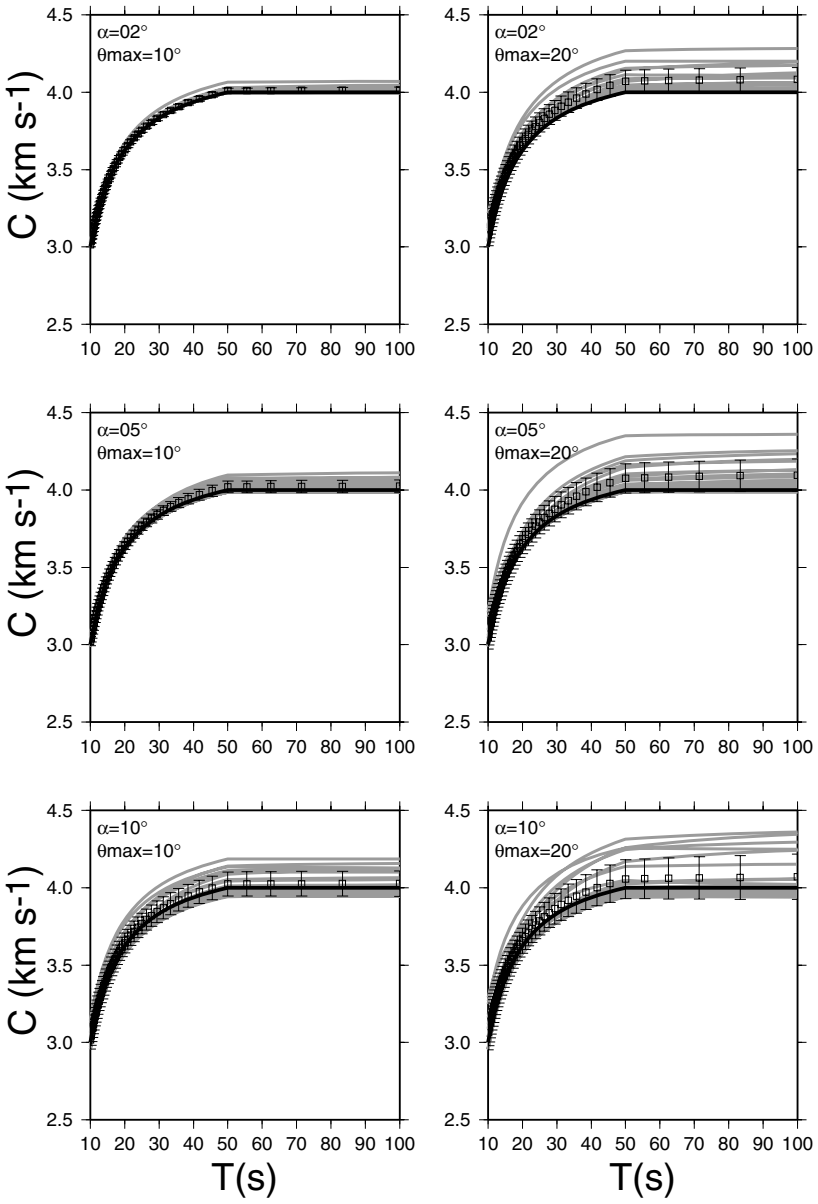

Figure 2. Apparent phase velocities (grey lines) using 20 realizations of deviations from great-circle propagation. The reference (structural velocity) dispersion curve is shown by the solid black line and the error bars show the average apparent dispersion curve and associated standard deviation. The difference between the structural and average apparent velocities is of the order of 0.5 per cent in the left column and 2 per cent in the right one. In the upper left corner of each plot is the value of α (the angle in degrees between the station profile and the great-circle) and $\theta_{\max}$ (the upper limit of the deviation in degrees from the great-circle path).

the slowness vector. In the presence of great-circle deviations, this projection is no longer valid and the velocity calculated by eq. (1) no longer yields the real velocity C but an apparent velocity C_{app}.

In this and the following sections we use the term 'structural velocity' for the phase velocity defined by the medium within which the waves propagate (C in eq. 1) We use the term 'apparent velocity' (C_{app}) for the velocity between two stations as measured with a two-station phase velocity measurement.

The ratio $R(f)$ at frequency f between $C_{app}(f)$ and $C(f)$ (in the absence of other sources of error) can be expressed as

$$R(\alpha, \theta(f)) = C_{app}(f)/C(f) = \cos(\alpha)/\cos(\theta(f) + \alpha), \qquad (2)$$

where θ is the (frequency dependent) deviation from the great-circle path. Fig. 1 shows $R(\alpha,\theta)$ for realistic values of α and θ. Even in the case where the station profile and the source–receiver great-circle are almost aligned ($\alpha < 5°$), the phase velocity errors can still be up to 5–10 per cent.

To estimate the variability of the resulting dispersion curves, and to compare that variability with error estimates in the following sections, Fig. 2 shows a series of dispersion curves obtained with different values of α and θ. In all calculations, we use a reference (structural velocity) dispersion curve $C(f)$ which is constant at 4 km s^{-1} for frequencies lower than 0.02 Hz, and decreases linearly from 4 km s^{-1} to 3 km s^{-1} for frequencies between 0.02 and

0.1 Hz. This simple dispersion curve ensures coverage of the range of wavelengths usually explored in lithospheric surface wave studies. In each plot α is constant; the values being 2° at the top, 5° at the centre and 10° at the bottom. To allow for the fact that deviations are generally not constant with frequency, θ varies linearly with frequency between $\theta(0.01\ \text{Hz})$ and $\theta(0.1\ \text{Hz})$, these two limits being chosen arbitrarily between $\pm\theta_{\max}$, where $\theta_{\max}$ takes the value of 10° (left column) and 20° (right column).

The systematic shift between the apparent velocities, averaged over 20 realizations, and the structural velocities is of the order of 0.5 per cent for $\theta_{\max} = 10°$ and 2–2.5 per cent for $\theta_{\max} = 20°$. The large variability of the great-circle deviation θ dominates the systematic shift to higher apparent velocities whereas increasing α introduces a higher error to each individual curve without significantly affecting the shift.

Note that this simulation does not by any means maximize the errors because the random selection of θ ensures that the mean value of θ is approximately 0°, and the mean absolute value of θ is of the order of $\theta_{\max}/2$. In field experiments of sufficient duration to record a large number of events, a typical maximum value of α would be of the order of 5°. It is not uncommon, however, during short experiments or when the station profile geometry is unfavourable, for the maximum value of α to reach 7°–8°. Our results show that, compared to the effect of θ, an increase in α does not have a catastrophic result if a high number of events from different epicentral areas (i.e. different values for θ) are used to produce the average apparent dispersion curve.

3 UNCORRELATED NOISE

In this section, we investigate the influence of phase perturbations induced by noise that is not correlated between stations, that is, noise generated by local sources. This kind of noise can be considered event independent. If the phase of uncorrelated noise was fully random and independent of frequency, it would be easy to suppress its effect through smoothing of the dispersion curve. In field data, however, the phase of the noise is not fully random and any individual event may have significant bias, which does not oscillate strongly with frequency. As the uncorrelated noise varies strongly both in time and space, we cannot assume that it has any particular phase characteristics. We consequently use constant amplitude noise with random phases, which provides us with the potential size of the errors on the dispersion curve caused by uncorrelated noise.

To explore the influence of uncorrelated noise, we calculate the displacement of a plane acoustic wave at two sensors separated by a distance $D = 200$ km. The medium is characterized by the same dispersion curve as in the previous section and the profile is parallel to the propagation direction.

In the plane and for a given frequency f, a plane acoustic wave can be calculated at any point (x, y) by

$$\vec{u}(x, y) = \vec{\nabla}\phi, \tag{3}$$

where u is the displacement and $\phi(x,y)$ is the scalar wave-potential:

$$\phi(x, y) = A \exp\left(ik_x x + ik_y y - i\frac{2\pi}{f}t + i\phi_0\right). \tag{4}$$

k_x and k_y are the wavenumbers in directions x and y and ϕ_0 is the wave phase at $t = 0$ and $(x, y) = (0, 0)$.

Note that ϕ traditionally is used both for the wave potential and for the phase of a wave, but since we no longer need to refer to the wave potential, ϕ will be used to designate phases in the remaining part of the paper.

We add random noise to the signals at the two stations in such a way that the amplitude of the noise divided by the amplitude of the signal is constant N in each calculation and the phase of the noise is fully random. We measure apparent phase velocities

$$C_{app}(f) = \frac{D}{\Delta t} \tag{5}$$

between the two stations by transforming the phase difference $\Delta\phi(f)$ of the two signals into a time delay Δt

$$\Delta t(f) = \frac{\Delta\phi(f) + M2\pi}{2\pi f}. \tag{6}$$

As the profiles are relatively short, $M = 0$ at low frequency. We estimate the value of M at successively higher frequencies by incrementing M by 1 every time an approximate 2π phase jump is encountered. This very simple method is likely to fail sometimes at high frequencies in the presence strong phase oscillations due to random noise. We, therefore, subsequently adjust the value of M so that the Δt falls within half a period of the time delay predicted by the apparent phase velocity averaged over all events. This procedure has to be carried out over one to two iterations, because the average apparent velocity changes slightly when corrections are applied to M.

In practice the signal-to-noise ratio is generally difficult to estimate for surface waves, mainly due to the temporal variability of the noise on broad-band stations, especially for temporary installations. The event-dependent frequency–time filtering often applied prior to phase velocity measurements further complicates the estimate of the signal-to-noise ratio. The required ratio will also depend on the station profile length as well as on frequency, because the influence of uncorrelated noise decreases with the ratio between profile length and wavelength. We here use noise levels of $N = 0.1$ and $N = 0.25$ to cover the range of realistically expected values in temporary field experiments.

Fig. 3 shows the average apparent velocity along a $D = 200$ km profile, using 20 noise realizations for each profile. Due to the randomness of the phase, the average apparent velocities are practically identical to the structural velocities when enough events are used. The number of events required to obtain a reliable dispersion curve will depend on the profile length and noise level. For a 200-km-long profile, the standard deviation overestimates the errors when 20 events are used, while the standard deviation and the error on the dispersion curve were comparable with as few as five events.

4 NON-PLANE INCOMING WAVES

In this section, we explore different station configurations and amplitudes of non-plane waves to determine how two-station apparent velocities behave in the presence of interfering incoming waves. In the numerical experiments we use the same homogeneous 'medium' as in the previous section. A plane acoustic wave of unit amplitude is incident from the north. To create a non-plane wavefield we use an approach similar to that of Friederich *et al.* (2000), which consists of introducing additional plane waves with independent arbitrary amplitudes and incidence angle to the main incoming wave. Each wave is calculated by eqs (3)–(4) and subsequently added to obtain the total wavefield. To cover the range of frequencies used for typical lithospheric studies we use frequencies between 0.01 and 0.1 Hz.

Numerical tests using between 10 and 100 additional waves to create the non-plane waves showed that only the total energy of

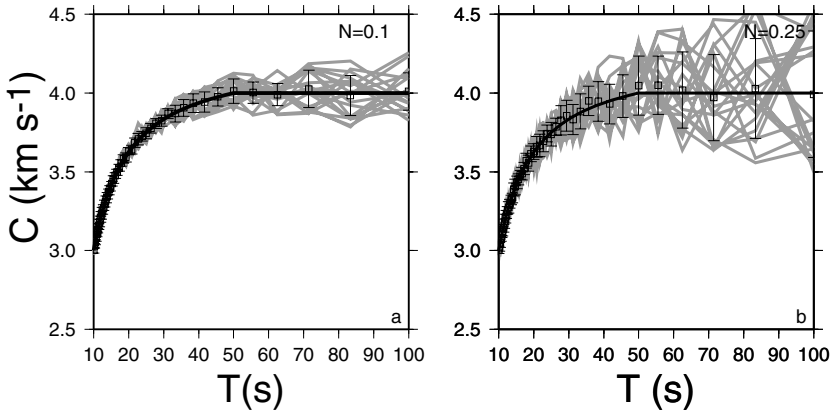

Figure 3. Apparent phase velocities (grey lines) along 200-km-long profiles using 20 noise realizations. The amplitude of the noise relative to the amplitude of the incoming wave is $N = 0.1$ (left) and $N = 0.25$ (right). The black line is the reference (structural velocity) dispersion curve and the error bars show the average apparent dispersion curve and associated standard deviation.

the additional waves compared to that of the main incoming wave determines the phase velocity errors (i.e. the difference between the apparent and the structural velocity). Consequently the number of waves over which this energy is spread has a negligible effect. We choose to follow Friederich *et al.* (2000) and use 50 plane waves to create the non-plane energy.

We measure apparent phase velocities $C_{app}(f)$ using the phase difference of the total wavefield between pairs of stations located D km apart on a N–S profile (see eqs 5 and 6). In the velocity calculation we ignore the contribution of other waves to the phase and as a result $C_{app}(f)$ may differ from the structural velocity $C(f)$. We will use the terminology suggested by Wielandt (1993) and define the 'dynamic phase velocity', at any point (x, y), as the apparent velocity along infinitely short profiles. $C_{app}(f)$ will in this section correspond to some integration of this dynamic phase velocity along the profile.

In this first calculation we choose a particularly simple model in which all random parameters (amplitude A, incidence angle β, and phase shift ϕ_0) of the 50 additional waves vary linearly with frequency. The values of these three parameters are determined randomly at 0.01 and 0.1 Hz, and they evolve linearly between these two frequencies. The intervals within which the random values are chosen is: $\beta \in [-\beta_{\max};\beta_{\max}]$ for the incidence angle (from the North); $\phi_0 \in [-\pi;\pi]$ for the phase shift; and $A \in [0;A_{\max}]$ for the amplitude. $A_{\max}$ is the maximum secondary wave amplitude divided by the amplitude of the main incident wave.

The addition of the secondary waves results in a wavefield with varying amplitude and dynamic velocity (see Fig. 1 in Friederich *et al.* 2000). For example at 0.02 Hz, and with $A_{\max} = 0.02$ the sum of the energy of the additional waves is approximately 0.4 per cent of that of the main wave. In this case the dynamic velocity within the area has minimum and maximum values of approximately 3.5 km s^{-1} and 4.5 km s^{-1}, that is, a variation of more than 10 per cent around the structural velocity of 4 km s^{-1}. These values show that non-plane effects can be catastrophic for phase velocity measurements. The question is how this translates into two-station apparent phase velocity measurements.

Fig. 4 shows $C_{app}(f)$ curves using three different profile lengths, and for 20 realizations in each plot. With $A_{\max} = 0.02$ the apparent velocity curves are stable up to at least a period of 100 s for the 200 km profile, that is, up to wavelengths twice the profile length. Due to our assumption that the events are independent, the apparent velocity curves scatter around the structural velocity. The realization with the highest difference between the dynamic velocity and the structural velocity (approximately 18 per cent) gives up to 2 per cent differences between apparent and structural velocities for the 200-km-long profiles. More importantly, the average difference in velocities is only up to 0.5 per cent for periods between 50 and 100 s.

These results are encouraging, as they tend to show that the average apparent dispersion curve is much more stable than the local values of the dynamic velocities, particularly when we use a sufficiently large number of uncorrelated events. However, we do not know the amplitude of the non-plane wavefield and it is not obvious how to reliably determine it. For example, if we estimate the total energy E_{total} in our simulations as the average over $301 \times 301 = 90\,601$ points evenly spaced in an area of $1200 \times 1200\,\text{km}^2$, E_{total} oscillates within 0.95–1.05 while the theoretical value lies around 1.005, depending on the realization.

Any such energy measurement on field data is very difficult as the station coverage is too poor to provide a reliable estimate. So far, the best estimate comes from Friederich *et al.* (1994). They pre-processed teleseismic broad-band records to extract the surface waves and subtracted the best-fitting plane wave from the resulting traces. The remaining average energy over the area was then attributed to non-plane energy, including uncorrelated noise. They showed that the ratio *En* of total non-plane energy to the plane wave energy increases strongly with frequency, and varies within approximately an order of magnitude for different earthquakes. The majority of their observations are located between two lines

$$\log En(f) = A \log(f) + B, \tag{7}$$

with $A = 2.4$ for the two lines, $B = 2.1$ for the lower line and 3.4 for the upper line. In the remaining part of this section, we base the estimations of non-plane energy on these observations. The upper line corresponds to *En* values of approximately 0.04 at 0.01 Hz and 0.21 at 0.02 Hz and which extrapolate to 10 at 0.1 Hz. Recalling that Fig. 4 corresponded to non-plane energy of 0.004, these observed values of non-plane energy must surely be catastrophic to any two-station measurements. The only positive point is that the non-plane energy decreases at long periods.

The amplitude of each of the 50 additional waves is calculated by assuming that each of them carries an amount of energy which is a

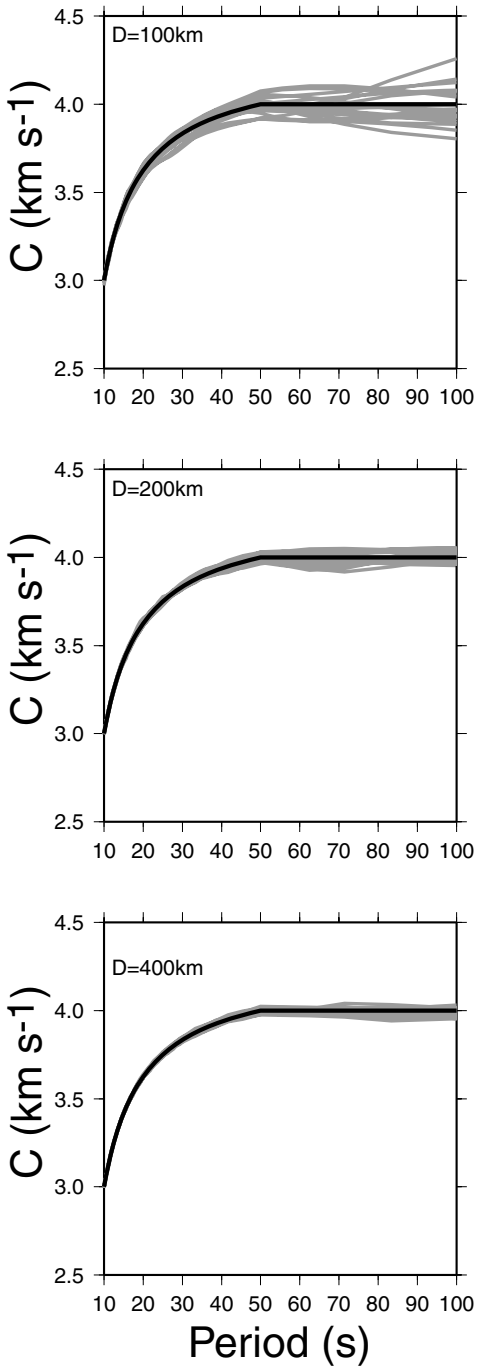

Figure 4. Apparent phase velocities (grey lines) measured along profiles that are 100 km (top), 200 km (centre) and 400 km (bottom) long. In each plot the apparent velocities correspond to 20 different realizations of non-plane waves, with $A_{\max} = 0.02$ and $\beta_{\max} = 180^\circ$. The black line is the reference (structural velocity) dispersion curve.

fiftieth of $En(f)$ where $En(f)$ is defined by

$$\log En(f) = 2.4 \log(f) + B. \quad (8)$$

For each additional wave, B is chosen randomly between 2.1 and 3.4. The apparent phase velocities calculated for 20 realizations are shown in Fig. 5(a) for additional waves coming from all directions ($-180^\circ < \beta < 180^\circ$) and in Fig. 5(b) for wave propagation within ($-90^\circ < \beta < 90^\circ$). Two different ranges of incidence directions of the additional waves were used because fundamental mode Rayleigh waves are mainly scattered in the forward direction, whereas higher modes and Love waves have a more complex diffraction pattern (e.g. Snieder 1986).

Even though the simulations using additional waves from all directions have the highest variations in dynamic phase velocities due to the rapidly oscillating amplitudes of the total wavefield, the use of the total phase difference between the two endpoints of the profiles tends to average out these extreme values. On the contrary, the 'forward scattering' case ($-90^\circ < \beta < 90^\circ$) has much slower variations in the wavefield and, therefore, smaller spatial oscillations of the dynamic velocity. These oscillations can be systematic along a profile, however, giving rise to dispersion curves that are completely outside any acceptable error bounds.

The standard deviation is up to approximately 4 per cent of the average apparent velocity, however, one must also keep in mind that the *smallest* errors govern the inversion of the dispersion curve, because dispersion curves are smooth in the period range considered. It is clear, however, that if the amount of non-plane energy is as strong as assumed here it will not be possible to extract any but the largest changes in structure, because any small lateral differences between two profiles will lie within the error bars.

Considering the errors, it is surprising that the average apparent velocity falls so close to the structural velocity. Our choice of 20 realizations or 'events' for each simulation may be overly optimistic: a typical 6–8-month summer experiment is often too short to have so many events for each profile, even though the two-station profiles most often are set in the direction of maximum seismicity.

Decreasing the number of events may still result in average apparent phase velocities close to the structural phase velocities. Fig. 6 shows the effect of decreasing the number of events to five (left column) or 10 (right column), in each case using additional waves from the same half-plane as the main wave (($-90^\circ < \beta < 90^\circ$, top), or from all directions ($-180^\circ < \beta < 180^\circ$, bottom). The variability of the average apparent dispersion curves corresponds approximately to the standard deviations of Fig. 5 when the number of events is as small as five.

Obviously these results depend strongly on profile length. The scaling with profile length is more complicated than it would appear in Fig. 4 because the amount of non-plane energy varies with frequency. Increasing the profile length simply decreases the scatter in the dispersion curves for each event, even if the decrease is not as simple as in Fig. 4. For 400-km-long profiles, the apparent phase velocity is always close to the structural phase velocity, within at most ± 1.8 per cent when the additional waves arrive from all directions and ± 2.5 per cent in the 'forward scattering' case. This means that even a single event gives a meaningful result in terms of the structural velocity, and averaging over just a few independent events will ensure that the apparent phase velocity is accurate within ± 0.5 per cent.

The case of decreasing profile lengths is more complex, because the profile length becomes comparable to the wavelength at increasingly shorter periods. For example, when the profile length is reduced to 100 km the error bars simply increase by a factor of 2–3 at long periods. However, at intermediate periods (20–50 s), the average apparent dispersion curve shows not only increased scatter, but also a systematic shift towards higher apparent velocities. The average apparent velocities has a maximum difference with the

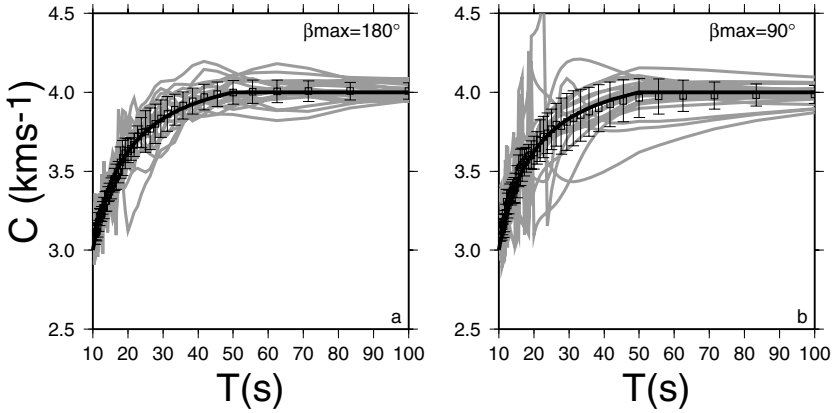

Figure 5. Apparent phase velocities (grey lines) measured for 20 realizations of additional plane waves using values for non-plane energy taken from Friederich *et al.* (1994). In the left plot the additional waves are incident from all directions ($\beta_{\max} = 180°$), and in the right plot they are incident from the same half-plane as the main wave ($\beta_{\max} = 90°$). The black line is the reference (structural velocity) dispersion curve and the error bars show the average apparent dispersion curve and associated standard deviation.

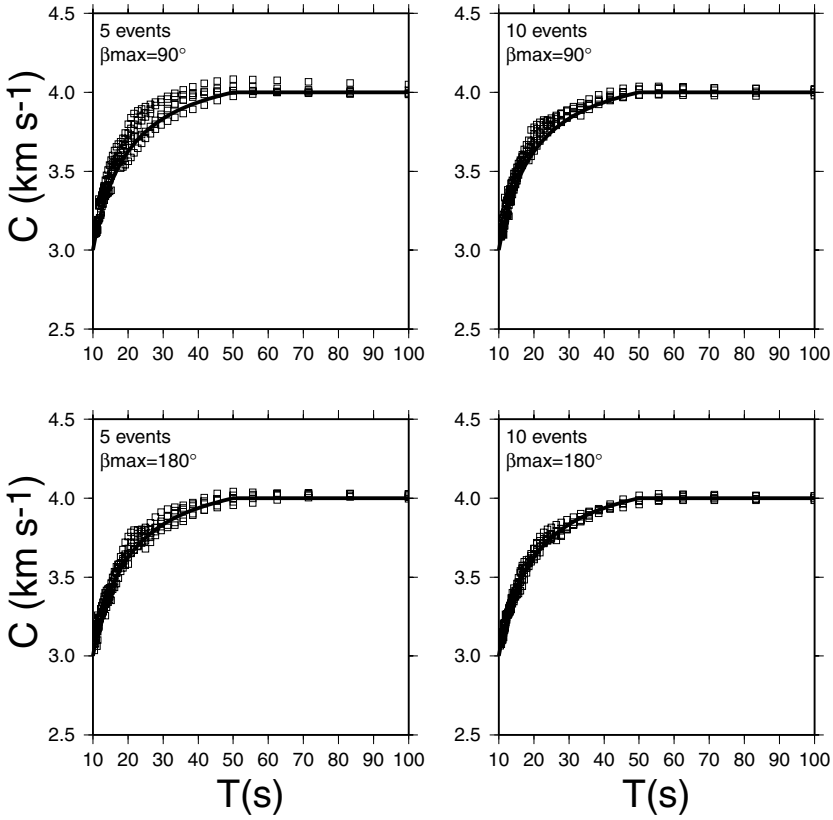

Figure 6. Average apparent phase velocities along 200-km-long profiles. In each plot five average curves are plotted (squares) and the parameters of the calculation are given in the top left corner of each plot. The five average apparent velocities are in each case obtained over five (left column) or 10 (right column) 'events'. The top of the figure corresponds to additional waves incident from the same half plane as the main wave ($\beta_{\max} = 90°$), and the bottom to additional events from all directions ($\beta_{\max} = 180°$). The amplitude of the additional events is randomly chosen as explained in the text. The black line is the reference (structural velocity) dispersion curve.

structural velocities of 0.15–0.2 km s^{-1} at approximately 25 s period where the total non-plane energy can be high as the plane energy. For many of the events, a simple 'polarization analysis' (consisting of rotating the records until the energy on the transverse component is minimal) shows that at intermediate periods the waves no longer propagate N–S between the stations. Consequently, the additional non-plane waves will locally result in a deviation of the wavefield from the great-circle path. This effect would systematically increase the apparent velocities (see Fig. 1). With the complexity of overlap between Rayleigh waves and the Love wave coda, it is questionable whether a polarization analysis could be used to correct for this effect. This implies that when the station profiles are short, some

off-profile stations should always be included in the array setup to be able to correct for the propagation direction.

5 CONCLUSIONS

Phase velocity measurements between two closely located stations exhibit significant errors and, as a consequence, we can only expect to retrieve large differences in earth structure between different station pairs.

Because non-plane energy is not necessarily the dominant source of error, it is possible, however, to obtain the structural velocity between two stations using data from a relatively small number of events. The errors induced by non-plane energy are no higher than those arising from uncorrelated noise and from off great-circle propagation in the case of 200-km-long profiles, and the errors decrease with increasing profile length.

These conclusions are based on the assumption that each event is dominated by event-independent non-plane energy, which is obviously incorrect if events from only the same epicentral area are used or if strong diffractions are created close to the seismic stations. It is not known whether teleseismic waves from the same direction but different epicentral distances have similar non-plane energy. To fully answer this question, full wave diffraction in realistically heterogeneous global models must be carried out. Such tests may soon be feasible (e.g. Chaljub *et al.* 2003). A partial answer can come from the calculation of great-circle deviations as was done by Cotte *et al.* (2000), who showed that even with smooth earth models, great-circle deviations can generally be expected to depend on both backazimuth and epicentral distance. This arises because the surface waves carry very different diffraction histories and the distortion of the wave fronts is consequently likely to vary for different epicentral areas. It is nevertheless unclear whether waves that cross heterogeneities close to the study area, but which have previously gone through different diffraction histories, will show systematically biased dispersion curves. In view of these uncertainties, methods that correct for non-plane energy should be used whenever the station configuration and the amount of data allow. Such methods also naturally make it possible to correct for deviations from great-circle propagation.

It is essential to have sufficient events from different epicentral areas to overcome the problems of non-plane waves. However, to obtain a sufficient number of epicentral areas for which the records can be used, it is sometimes necessary to relax the constraint that the alignment of great-circle and station profile must be almost perfect, and this may introduce additional errors due to off great-circle propagation. Errors due to off great-circle propagation may be significant even when the station profile—great-circle alignment is good. Such errors are of the same order of magnitude or even larger than those arising from non-plane waves, even when the profile is perfectly aligned with the great-circle.

Array analysis is necessary to correct for deviations from the great-circle propagation. Even though errors from non-plane energy may be smaller than initially assumed, some off-profile stations in otherwise linear broad-band arrays must be included if reliable results are to be obtained.

ACKNOWLEDGMENTS

The author gratefully acknowledges the Alexander von Humboldt Foundation for financing research at the GeoForschungsZentrum Potsdam and the University of Potsdam, Germany. Discussions with Wolfgang Friederich initiated this work and discussions with him and other colleagues have provided valuable input. Nicholas Arndt provided helpful comments for the final version of the paper. We thank the reviewers for constructive comments that helped to improve the manuscript.

REFERENCES

Alsina, D. & Snieder, R., 1996. Constraints on the velocity structure beneath the Tornquist-Teysseire Zone from beam-forming analysis, *Geophys. J. Int.,* **126,** 205–218.

Alsina, D., Snieder, R. & Maupin, V., 1993. A test of the great circle approximation in the analysis of surface waves, *Geophys. Res. Lett.,* **20,** 915–918.

Baumont, D., Paul, A., Zandt, G., Beck, S. & Pedersen, H.A., 2002. Lithospheric structure beneath the Central Andes based on surface wave dispersion, *J. geophys. Res.,* **107,** doi:10.1029/2001/JB00034.

Bruneton, M., Pedersen, H.A., Farra, V., Arndt, N.T., Vacher, P. & the SVEKALAPKO Seismic Tomography Working Group, 2004. Complex lithospheric structure under the central Baltic Shield from surface wave tomography, *J. geophys. Res.,* **109,** B10303.

Chaljub, E., Capdeville, Y. & Vilotte, J.-P., 2003. Solving elastodynamics in a fluid-solid heterogeneous sphere: a parallel spectral element approximation on non-conforming grids, *J. Comp. Phys.,* **187,** 457–491.

Cotte, N., Pedersen, H.A., Campillo, M., Farra, V. & Cansi, Y., 2000. Off-great-circle propagation of intermediate-period surface waves observed on a dense array in the French Alps, *Geophys. J. Int.,* **142,** 825–840.

Du, Z. & Foulger, G.R., 2004. Surface wave waveform inversion for variation in upper mantle structure beneath Iceland, *Geophys. J. Int.,* **157,** 305–314.

Friederich, W., 1998. Wave-theoretical inversion of teleseismic surface waves in a regional network: phase velocity maps and a 3-D upper mantle shear wave velocity model for southern Germany, *Geophys. J. Int.,* **132,** 203–225.

Friederich, W., Wielandt, E. & Stange, S., 1994. Non-plane geometries of seismic surface wavefields and their implications for regional surface-wave tomography, *Geophys. J. Int.,* **119,** 931–948.

Friederich, W., Hunzinger, S. & Wielandt, E., 2000. A note on the interpretation of seismic surface waves over three-dimensional structures, *Geophys. J. Int.,* **143,** 335–339.

Gregersen, S., 1978. Possible mode conversion between Love and Rayleigh waves at a continental boundary, *Geophys. J.R. astr. Soc.,* **54,** 121–127.

Kennett, B.L.N., 1984. Guided-wave propagation in laterally varying media. I. Theoretical development, *Geophys. J.R. astr. Soc.,* **79,** 235–255.

Kennett, B.L.N. & Yoshizawa, K., 2002. A reappraisal of regional surface wave tomography, *Geophys. J. Int.,* **150,** 37–44.

Lander, A.V. & Levshin, A.L., 1989. Recording, identification and measurement of surface wave parameters, in *Seismic Surface Waves in Laterally Inhomogeneous Earth*, ed. Keilis-Borok, V.I., Kluwer Publ., Dordrecht.

Laske, G. & Masters, M., 1996. Constraints on global phase velocity maps by long-period polarization data, *J. geophys. Res.,* **101,** 16 059–16 075.

Li, A., Forsyth, D.W. & Fischer, K., 2003. Shear velocity structure and azimuthal anisotropy beneath eastern North America from Rayleigh wave inversion, *J. geophys. Res.,* **108,** 2362, doi:10.1029/2002JB002259.

Marquering, H., Snieder, R. & Nolet, G., 1996. Waveform inversions and the significance of surface wave modes coupling, *Geophys. J. Int.,* **124,** 258–278.

Maupin, V., 1988. Surface waves across 2-D structures: a method based on local modes, *Geophys. J. Int.,* **93,** 173–185.

Maupin, V., 2001. A multiple-scattering scheme for modelling surface wave propagation in isotropic and anisotropic three-dimensional structures, *Geophys. J. Int.,* **146,** 332–348.

McGarr, A. & Alsop, L.E., 1967. Transmission and reflection of Rayleigh waves at vertical boundaries, *J. geophys. Res.,* **72,** 2169–2180.

Nolet, G., 1987. Seismic wave propagation and seismic tomography, in *Seismic Tomography*, pp. 1–23, ed. Nolet, G., Reidel, Dordrecht.

Pedersen, H.A., Maupin, V. & Campillo, M., 1996. Wave diffraction in multilayered media with the indirect boundary element method: application to 3-D diffraction of long-period surface waves by 2-D lithospheric structures, *Geophys. J. Int.,* **125,** 545–558.

Pollitz, F., 1999. Regional velocity structure in northern California from inversion of scattered seismic surface waves, *J. geophys. Res.,* **104,** 15 043–15 072.

Snieder, R., 1986. 3D linearized scattering of surface waves and a formalism for surface wave holography, *Geophys. J. R. astr. Soc.,* **84,** 581–605.

Wielandt, E., 1993. Propagation and structural interpretation of non-plane waves, *Geophys. J. Int.,* **113,** 45–53.

Woodhouse, J.H. & Wong, Y.K., 1986. Amplitude, phase and path anomalies of mantle waves. *Geophys. J. R. astr. Soc.,* **87,** 753–773.

Yanovskaya, T.B., 1996. Ray tomography based on azimuthal anomalies, *Pure appl. Geophys.,* **148,** 319–336.

Yoshizawa, K. & Kennett, B.L.N., 2002. Determination of the influence zone for surface waves, *Geophys. J. Int.,* **149,** 118–133.

Yoshizawa, K., Yomogida, K. & Tsuboi, S., 1999. Resolving power of surface wave polarization data for higher-order heterogeneities, *Geophys. J. Int.,* **138,** 205–220.